Inorganic Chemistry

pubs.acs.org/IC Article

Predicting $\sigma^0\pi^2$ Carbene-Mediated Hydroboration and Bis-carbene Functionalization of Dinitrogen

Shicheng Dong, Jun Yan, Weitang Li, Zhigang Shuai, and Jun Zhu*

Cite This: *Inorg. Chem.* 2025, 64, 10115−10126 Read Online

ACCESS | Metrics & More | Article Recommendations | Supporting Information

ABSTRACT: Although the carbene-catalyzed N_2 fixation process had been investigated by scientists for decades prior to borylene species, the interest in the carbene-mediated N_2 activation process has drawn less attention than that of borylene species in the past few years, especially unique $\sigma^0\pi^2$ carbenes. Herein, we demonstrate the important role of unique $\sigma^0\pi^2$ carbenes in the 1,1-hydroboration and bis-carbene functionalization of N_2 using density functional theory calculations. Both being kinetically and thermodynamically favorable, the reaction barriers are as low as 13.7 and 16.6 kcal/mol, respectively. Additionally, such a $\sigma^0\pi^2$ carbene can also achieve a series of X−H insertion reactions (X = H, CH_3, Bpin, or SiH_2Ph), with activation energies ranging from 8.2 to 15.3 kcal/mol. Our findings highlight a strong potential of carbenes with $\sigma^0\pi^2$ electronic configuration in N_2 activation and its versatile transformations, providing valuable insights into main-group-element-mediated N_2 activation chemistry.

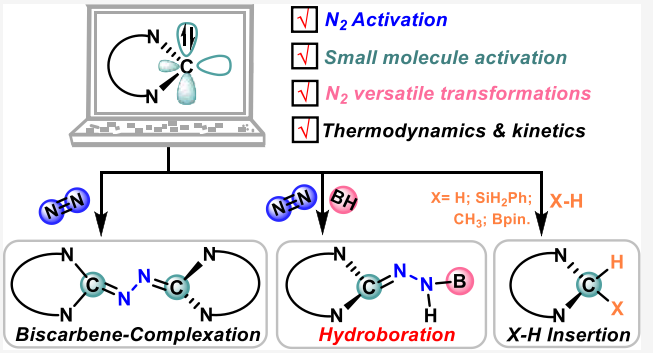

INTRODUCTION

Dinitrogen (N_2), the most abundant and "cheapest" source of nitrogen, is virtually inexhaustible. However, due to its extreme inertness, it is notoriously difficult to activate and transform.[1] Undoubtedly, achieving the activation and direct transformation of N_2 under mild conditions represents a significant scientific challenge that urgently needs to be addressed.[2] In nature, nitrogenase enzymes can achieve N_2 conversion under mild conditions;[3] however, industrially, the Haber−Bosch process remains the predominant method for converting N_2 into ammonia (NH_3) using transition metal (TM) catalysts, primarily for fertilizer production.[4,5] This process accounts for approximately 2% of global energy consumption annually.[6] To date, almost all TM-N_2 complexes across the periodic table have been reported, thanks to the synergistic interaction between occupied and unoccupied d-orbitals of TMs (Figure 1a).[7−17] Besides metal catalysts, nonmetallic approaches to N_2 activation offer an alternative solution.[18−22] Recently, Branuschweig and co-workers demonstrated that by modifying the electronic environment of boron atoms stabilized by CAAC [(CAAC = cyclic (alkyl)(amino)-carbene][23] ligands, it is possible to achieve B-center binding,[24] reduction, dimerization,[25] and direct protonation of N_2.[26,27] This landmark work has laid the foundation for subsequent research into main-group-element-mediated N_2 activation,[28−30] including species such as beryllium,[31] low-valent alkaline earth (Ca[32] and Mg[33]) metal species, substituted boranes,[34,35] and divalent boron radicals.[36]

Carbenes, as highly reactive species, play a crucial role in both TM-catalysis and main-group chemistry.[37−42] Since the observation of N_2 exchange in diazomethane, carbene species have been considered excellent candidates for the direct construction of C−N bonds in nitrogen-containing organic compounds. In 1964, Moore and co-workers discovered that under matrix conditions, carbenes generated from the photolysis of diazomethane could reversibly bind to N_2,[43] a finding confirmed by isotopic labeling and later supported by mass spectrometry and infrared spectroscopy evidence from Shilov et al.[44] Concurrently, Braun, Herzberg, and Eder demonstrated that pressure is a key factor influencing the binding of singlet and triplet carbenes to N_2.[45] Thereafter, Zollinger et al. showed that, under solution conditions, only those organic species with a strong electrophilic character (i.e., possessing empty s-orbitals) and capable of effective π-electron feedback and donation can bind to N_2.[46] They also highlighted that overcoming the rapid intersystem crossing between singlet and triplet states enhances the reactivity of carbenes with N_2 in solution. On the other hand, theoretical chemists have also maintained a keen interest in the reactions between carbenes

Received: February 15, 2025
Revised: April 8, 2025
Accepted: April 24, 2025
Published: May 9, 2025

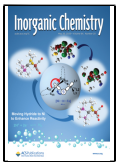

https://doi.org/10.1021/acs.inorgchem.5c00726
Inorg. Chem. 2025, 64, 10115−10126

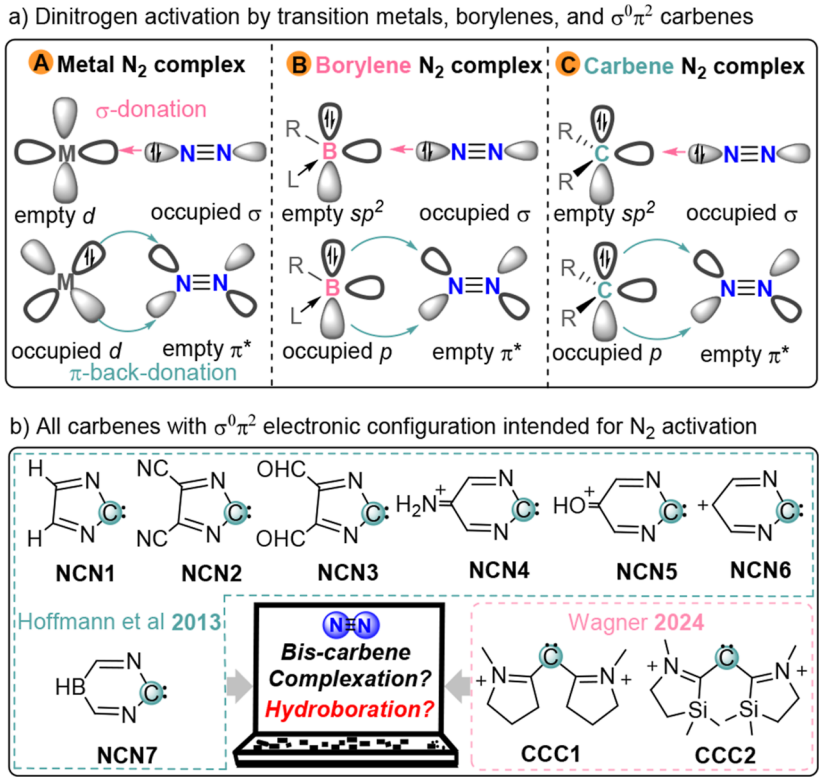

Figure 1. (a) N_2 activation by transition metals, borylenes, and $\sigma^0\pi^2$ carbenes. (b) All carbenes with a $\sigma^0\pi^2$ electronic configuration intended for N_2 activation.

and N_2. In 2003, Akasaka et al. demonstrated that the decomposition products of diazo-compounds can be classified as carbenes, diazo intermediates, or mixtures thereof, depending on the substituents on the substrate.[47] In 2012, Kim and co-workers showed through theoretical calculations that the cyclic diphosphinocarbenes (PHC) exhibit promising characteristics as an efficient catalyst for catalyzing N_2 to NH_3, attributed to the strong electron-donating ability of the carbene carbon atom.[48] Miliordos' research indicated that carbene pair with $\sigma^1\pi^1$ ground states can still activate N_2 using their excited $\sigma^2\pi^0$ states upon a perpendicular approach.[49] Meanwhile, similar studies on the binding of carbene carbon atoms with N_2 have also been reported.[50] In 2021, Lee's studies revealed that the large interaction energy between the SOMOs of anionic cyclic amino carbene radicals and the antibonding orbitals of N_2 is a critical factor for the low reaction barrier of N_2 by these carbenes.[51] Additionally, inspired by the excellent performance of frustrated Lewis pairs (FLPs) in small molecule activation,[52] Zhu's group designed a series of "carbene-boron" type FLPs, predicting thermodynamically and kinetically favorable N_2 activation, which provides new insights into N_2 fixation chemistry.[53−58] Their research also emphasized strategies involving molecules with dual Lewis acidity sites for N_2 activation, such as boron-substituted fluorene frameworks[59] and B_4N_2 inorganic benzene.[60]

Despite the early synthesis of the first $\sigma^0\pi^2$-configured carbene by Maier and Endres in 1999 through reversible photolysis of 2H-imidazole-2-ylidene[61] and the subsequent design strategy proposed by Borden and Hoffmann in 2013 to introduce sp^2-hybridized nitrogen atoms adjacent to the cyclic carbene carbon,[62] thereby destabilizing its σ-orbitals and stabilizing its $2p_\pi$-orbitals, significant experimental progress in isolating such carbenes was not achieved until very recently. Inspired by the previous work,[63] Liu's group successfully isolated a rhodium-coordinated cyclic diphosphinocarbene crystal, marking a major breakthrough in $\sigma^0\pi^2$-configured carbene chemistry.[64] Subsequently, our group predicted via computational modeling that $\sigma^0\pi^2$-configured carbenes could activate N_2 and achieve hydroboration of the coordinated N_2, highlighting the strong potential of these unique electron configurations in N_2 activation.[65] However, reports on the activation of N_2 by $\sigma^0\pi^2$-configured carbenes remain extremely scarce, and studies on the diverse transformations of coordinated N_2 are relatively limited.[66] To further explore the possibilities in this field, we conducted systematic research to uncover the unique role of $\sigma^0\pi^2$ carbenes in N_2 activation and its versatile transformations. This work seeks to address the current gaps and provide new insights into promising applications of these special carbene species (Figure 1b).

COMPUTATIONAL METHODS

According to the literature, the M06-2X[67] functional is highly reliable for calculations involving organic systems.[68] Therefore, all model molecules were fully optimized and subjected to frequency calculations using the Gaussian 16 (A.03) software package[69] under gas phase at the (U)M06-2X(D3)[70]/def2-SVP[71] level of theory. Additionally, the stability of wave functions for all optimized structures and transition states was verified using the "stable = opt" keyword. All optimized model molecules exhibited no imaginary frequencies, while the transition states possessed exactly one imaginary frequency. Furthermore, the accuracy of the two lower-energy structures connected by each transition state was confirmed using intrinsic reaction coordinate calculations.[72,73] Single-point energy calculations were performed using the (U)M06-2X(D3)/def2-TZVP[74,75] level. The Gibbs energy (ΔG) at 298.15 K was calculated using the formula $\Delta G = \Delta(E + G_{ZPE})$, where G_{ZPE} represents the Gibbs energy correction obtained from the (U)M06-

https://doi.org/10.1021/acs.inorgchem.5c00726
Inorg. Chem. 2025, 64, 10115−10126

Table 1. Gibbs Energies (ΔG_1: The Gibbs Energy Changes of the N_2 Fixation; ΔG_2: The Gibbs Energy Changes of the Bis-carbene Complexation. Both ΔG_1 and ΔG_2 Are Calculated Based on R. Unit: kcal/mol) for N_2 Activation via $\sigma^0\pi^2$ Carbenes. Comparison of Relative Electronic Energies ($\Delta E_{ST} = E_{Triplet} - E_{Singlet}$, kcal/mol) for $\sigma^0\pi^2$ Carbenes in Different Spin States

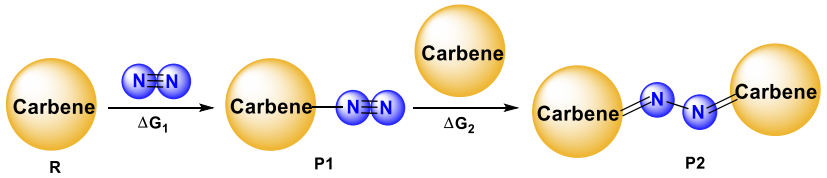

entry	NCN1	NCN2	NCN3	NCN4	NCN5	NCN6	NCN7	CCC1	CCC2
ΔE_{ST}	+1.0	+1.4	+7.9	+19.5	+33.5	+41.0	+20.7	−9.0	+13.8
ΔG_1	−15.3	−19.7	−12.3	−8.1	−6.8	−0.8	+10.5	−6.0	+20.7
ΔG_2	−66.5	−61.0	−49.2	+36.7	+60.2	NA	−1.5	+140.9	+169.1

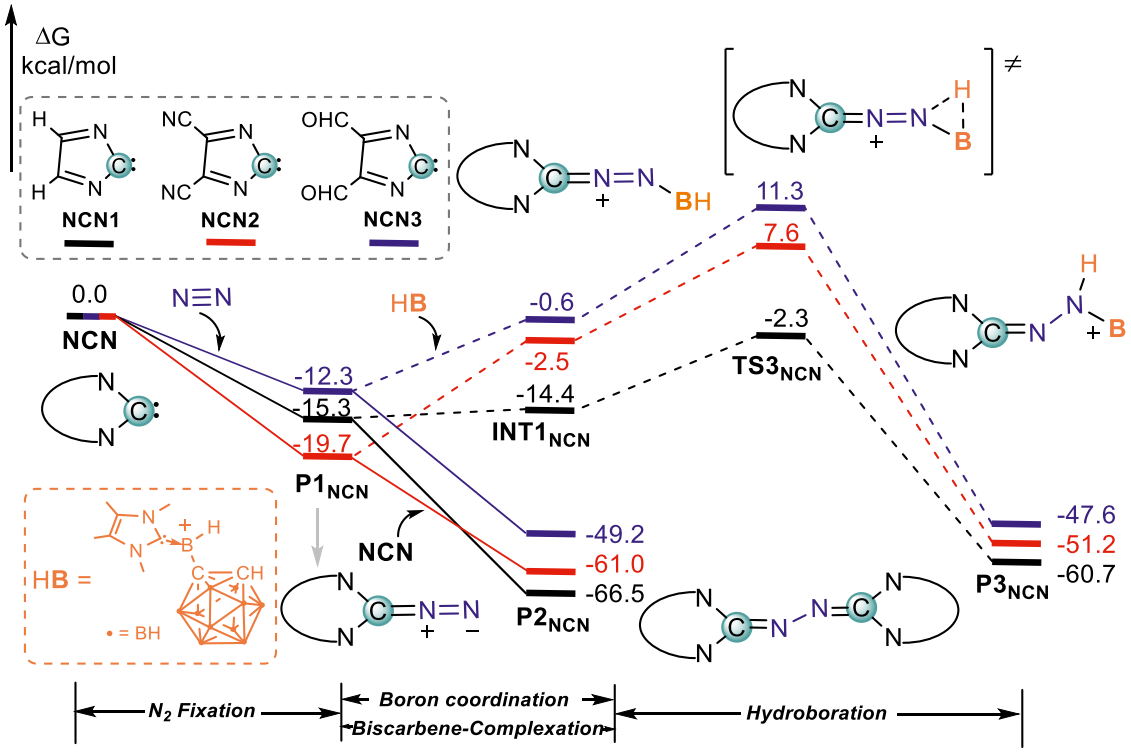

Figure 2. Gibbs energy (kcal/mol) profiles for the dinitrogen activation by five-membered cyclic $\sigma^0\pi^2$ carbenes (**NCN1**, **NCN2**, and **NCN3**).

2X(D3)/def2-SVP method and the electronic energy E is derived from single-point energy calculations at the (U)M06-2X(D3)/def2-TZVP level. To further validate the reliability of the computational methods, geometry optimizations were also conducted using the higher-precision (U)M06-2X(D3)/def2-TZVP method for comparison. The corresponding results were found to be almost identical to those obtained at the (U)M06-2X(D3)/def2-TZVP//(U)M06-2X(D3)/def2-SVP level, thus confirming the consistency and reliability of the chosen computational method. Density matrices of natural atomic orbitals used for Wiberg bond indices (WBI),[76] principal interacting orbital (PIO),[77,78] and natural population analysis (NPA) were obtained using the NBO 7.0 program[79] at the M06-2X(D3)/def2-SVP level. PIO analyses were performed using the PIO software available at https://github.com/jxzhangcc/PIO. Aromaticity indices, including nucleus-independent chemical shifts (NICS)[80] and anisotropy of the current-induced density (ACID),[81] were also computed at the M06-2X-D3/def2-SVP level. Also, viewing of optimized structures and rendering of various orbitals (FMO, PIO, PIMO) were performed using the CYLview[82] and the VMD,[83] respectively. Interaction region indicator (IRI)[84] analysis was conducted using the Multiwfn[85] program.

RESULTS AND DISCUSSION

Previous studies have shown that $\sigma^0\pi^2$-configured carbenes may be more favorable for N_2 activation. This could be attributed to the σ-type lowest unoccupied molecular orbital (LUMO) of $\sigma^0\pi^2$ carbenes, which can more readily accept electrons from the 2p orbitals of N atoms in N_2, while simultaneously occupied $2p_\pi$ electrons on the carbene carbon are donated back to the π^* orbitals of N_2 (Figure 1a).[49] Figure 1b lists the nine model molecules used in this work. Research by Borden, Hoffmann, and Wagner[86] has indicated that these molecules exhibit a $\sigma^0\pi^2$ electronic configuration, serving as models to investigate whether all $\sigma^0\pi^2$-configured carbenes can achieve N_2 activation. As shown in Table 1, the thermodynamics of reactions between these $\sigma^0\pi^2$ carbenes and N_2 are not uniformly favorable. Specifically, (a) for five-membered (5MR) cyclic $\sigma^0\pi^2$ carbenes (**NCN1**, **NCN2**, and **NCN3**), both the N_2 fixation (coordination) and bis-carbene-complexation processes exhibit negative Gibbs energy changes (ΔG), indicating thermodynamically favorable reactions. (b) In the

https://doi.org/10.1021/acs.inorgchem.5c00726
Inorg. Chem. 2025, 64, 10115−10126

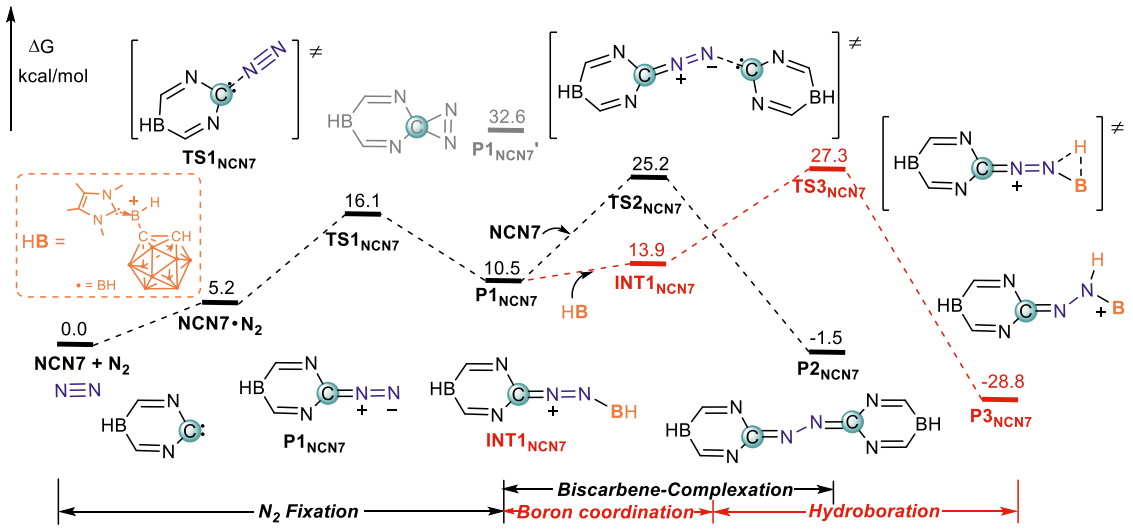

Figure 3. Gibbs energy (kcal/mol) profiles for the dinitrogen activation by six-membered cyclic $\sigma^0\pi^2$ carbene **NCN7**.

case of six-membered (6MR) cyclic $\sigma^0\pi^2$ carbenes (**NCN4**, **NCN5**, **NCN6**, **NCN7**), the first three carbene models (**NCN4**, **NCN5**, **NCN6**) show negative ΔG values for N_2 coordination but exhibit thermodynamically unfavorable conditions for the bis-carbene-complexation process. Conversely, **NCN7** behaves oppositely, where the formation of bis-carbene products is exergonic. (c) Although coordination with N_2 stabilizes the acyclic $\sigma^0\pi^2$ carbene **CCC1**, the subsequent bis-carbene functionalization remains endergonic. Moreover, highly positive ΔG values indicate that both N_2 coordination and bis-carbene-complexation are thermodynamically unfavorable for **CCC2**. The calculation results of ΔE_{ST} indicate that the ground states of carbenes with unique electronic configurations, except for **CCC1**, are all singlet states.

It is well-known that a comprehensive evaluation considering both thermodynamic and kinetic feasibility serves as the criterion for determining whether a reaction can be feasible. Next, we systematically investigate the detailed kinetic processes of the reactions between N_2 and the three classes of $\sigma^0\pi^2$-configured carbenes discussed above.

5MR $\sigma^0\pi^2$ Carbenes. As illustrated in Figure 2, the coordination of 5MR-cyclic $\sigma^0\pi^2$ carbenes (**NCN1**, **NCN2**, and **NCN3**) with N_2 results in the formation of corresponding carbene-N_2 (η^1-N_2) adducts $\mathbf{P1}_{NCN1-3}$. Subsequently, the terminal nitrogen atom continues to react with another carbene molecule, forming thermodynamically more stable dicarbene (μ-η:$^1\eta^1$-N_2) products $\mathbf{P2}_{NCN1-3}$. Interestingly, kinetic calculations indicate that these processes are barrierless, supported by potential energy surface scan results (Figures S1 and S2). Inspired by previous research, we investigated the hydroboration process of the η^1-N_2 adducts $\mathbf{P1}_{NCN1-3}$. Results show that the unsubstituted $\sigma^0\pi^2$ carbene **NCN1** undergoes two steps, boron coordination (Figure S3) and 1,2-hydrogen migration, to form the most thermodynamically (−60.7 kcal/mol) and kinetically ($\Delta G^{\ddagger}$ = 13.0 kcal/mol) favorable product $\mathbf{P3}_{NCN1}$. Notably, due to the higher thermodynamic stability of $\mathbf{P1}_{NCN3}$ (−19.7 kcal/mol), its hydroboration exhibits a slightly higher reaction barrier ($\Delta G^{\ddagger}$ = 27.3 kcal/mol), suggesting that the corresponding transformation is not likely to occur at room temperature.

6MR $\sigma^0\pi^2$ Carbenes. As shown in Figures S4 and 3, similar to the 5MR-cyclic carbenes, the reactions begin with the coordination of 6MR-cyclic $\sigma^0\pi^2$ carbenes (**NCN4**, **NCN5**, **NCN6**, **NCN7**) with N_2, forming the corresponding η^1-N_2 adducts $\mathbf{P1}_{NCN4-7}$. These intermediates then react further with another carbene molecule to form μ-η:$^1\eta^1$-N_2 products $\mathbf{P2}_{NCN4-7}$. However, computational results presented in Figure S4 indicate that for **NCN4**−**NCN6**, the formation of both bis-carbene products and hydroboration products is thermodynamically (+15.4 to +60.2 kcal/mol) and kinetically (61.7 to 81.4 kcal/mol) unfavorable. Surprisingly, the reaction of **NCN7** with N_2 yields bis-carbene and hydroboration products that are thermodynamically favorable, with ΔG values of −1.5 and −28.8 kcal/mol, respectively. Moreover, while the slightly higher activation energies ($\Delta G^{\ddagger}$ = 25.2 kcal/mol and $\Delta G^{\ddagger}$ = 27.3 kcal/mol) present a challenge, there is potential for modulation. As shown in Table S1, to further explore the possibility of modulating the activation of N_2 by **NCN7**, a series of substituents (Me, Ph, C_6F_5, ^{t}Bu, $SiMe_3$, F, Cl, CN, CF_3, OMe, BMe_2, NMe_2, PMe_2, and PMe_3) were used to replace the hydrogen on the boron atom of **NCN7**. The results indicate that the ΔG (ΔG_1 for N_2 coordination and ΔG_2 for bis-carbene functionalization) ranges from −1.4 to +13.0 kcal/mol and −44.0 to +54.2 kcal/mol, respectively. Notably, when the hydrogen on the boron atom is replaced by π-electron-donating groups (such as NMe_2, OMe, F, Cl, PMe_2, etc.), the thermodynamic tendency for the new $\sigma^0\pi^2$ carbenes to react with N_2 improves significantly, with ΔG_2 values ranging from −44.0 to −14.8 kcal/mol. Especially when the substituent is NMe_2, the reaction exhibits the most favorable thermodynamics (ΔG_1 = −1.4 kcal/mol, ΔG_2 = −44.0 kcal/mol), in sharp contrast to an originally endergonic ΔG_1. Further aromaticity analysis reveals that slight destabilization of $\sigma^0\pi^2$ carbene **NCN7R** is a crucial factor in reversing the thermodynamics of the reaction. Specifically, the $NICS(1)_{ZZ}$ value of **NCN7R** becomes less negative from −29.7 ppm in **NCN7** to −20.2 ppm. Additionally, the ACID plots with clockwise ring currents suggest aromaticity in both **NCN7R** and **NCN7** (Figures S5 and S6). Meanwhile, carbenes with stronger bonds tend to exhibit higher deformation energies and lower reactivity, as shown by the comparison of ν_{C-N} (**NCN7**, 373.6 cm^{-1}) > ν_{C-N} (**NCN7R**, 362.7 cm^{-1}).

Subsequently, a detailed kinetic analysis was conducted on the thermodynamically optimal carbene **NCN7R** reacting with

https://doi.org/10.1021/acs.inorgchem.5c00726
Inorg. Chem. 2025, 64, 10115−10126

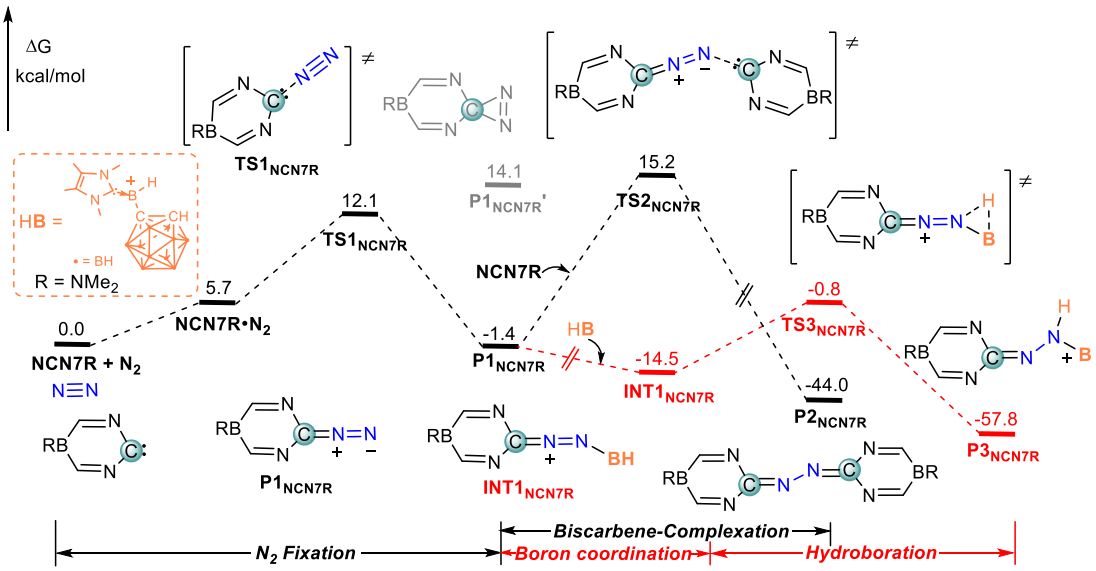

Figure 4. Gibbs energy (kcal/mol) profiles for the dinitrogen activation by $\sigma^0\pi^2$ carbene **NCN7R**.

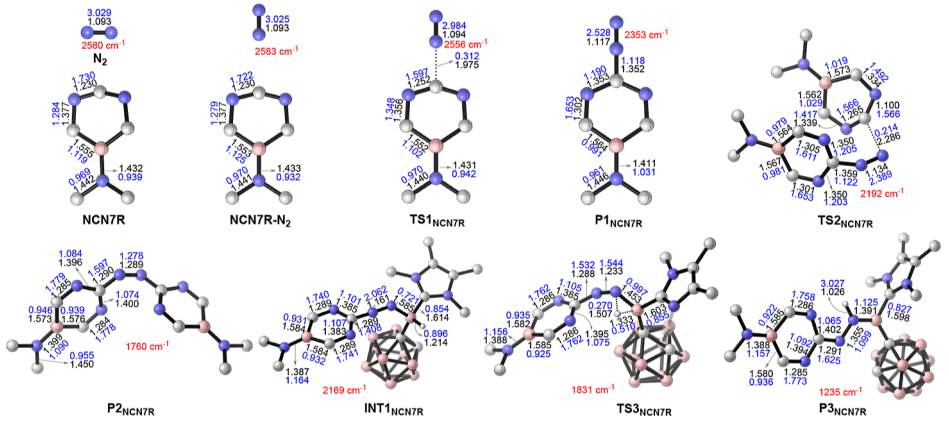

Figure 5. Optimized geometries of transition states and key intermediates for the N_2 activation by $\sigma^0\pi^2$ carbene **NCN7R**. Distances (black) are in Å. Wiberg bond indexes (blue) and ν_{NN} (red) in cm^{-1} are shown in the geometries.

N_2. As presented in Figure 4, compared to the parent **NCN7**, the reaction barriers corresponding to the transition states for both the N_2 coordination step and the bis-carbene-complexation step are reduced for carbene **NCN7R** by 4.0 kcal/mol ($\Delta G_1^{\ddagger}$ = 12.1 kcal/mol) and 8.6 kcal/mol ($\Delta G_2^{\ddagger}$ = 16.6 kcal/mol), respectively. This indicates that the bis-carbene functionalization reaction of **NCN7R** with N_2 is also kinetically feasible. Furthermore, computational results indicate that the hydroboration of N_2 induced by **NCN7R** becomes both thermodynamically and kinetically favorable. Specifically, $\mathbf{P1}_{\mathbf{NCN7R}}$ coordinates with the Lewis acid HB {[$IMe_4B(H)$-Cb][$B(C_6F_5)_4$], IMe_4 = 1,3,4,5-tetramethylimidazol-2-ylidene, Cb = *o*-carboran-1-yl)}[87] to form a more thermodynamically stable intermediate $\mathbf{INT1}_{\mathbf{NCN7R}}$, with a ΔG of −14.5 kcal/mol, which can be attributed to the formation of a "push−pull"[88] electronic effect along the "carbene → N → BH" axis. Subsequently, intermediate $\mathbf{INT1}_{\mathbf{NCN7R}}$ proceeds through transition state $\mathbf{TS3}_{\mathbf{NCN7R}}$, overcoming a reaction barrier of 13.7 kcal/mol to form hydroboration product $\mathbf{P3}_{\mathbf{NCN7R}}$, releasing 57.8 kcal/mol of energy. The reaction barrier for this process is reduced by 13.6 kcal/mol compared to the parent compound, highlighting the significant contribution of the substituent on boron to the kinetics of the reaction. Additionally, as shown in Figures S7 and S8, potential energy surface scan results indicate that the coordination of HB is also a barrierless process. Meanwhile, as shown in Figure S9, the results from direct optimization calculations using the higher-precision (U)M06-2X(D3)/def2-TZVP method further confirm the accuracy of the selected computational method.

The analysis of the geometric structures of key intermediates, transition states, and products throughout the reaction process indicates that the N−N bond length (d_{NN}) of the N_2 fragment gradually elongates, the bond order progressively decreases, and the vibration frequency (ν_{NN}) steadily diminishes. These observations provide compelling evidence for the feasibility of N_2 activation by the $\sigma^0\pi^2$ carbene **NCN7R**. Specifically, as illustrated in Figure 5, with the formation of η^1-N_2-type product $\mathbf{P1}_{\mathbf{NCN7R}}$ from N_2 and **NCN7R** and subsequently μ-η:$^1\eta^1$-N_2-type product $\mathbf{P2}_{\mathbf{NCN7R}}$, the changes in the N−N bond length are as follows: 1.093 Å → 1.117 Å → 1.289 Å (Δd_{NN} = 0.196 Å). Concurrently, the vibration frequencies change from 2580 cm^{-1} to 2353 cm^{-1} to 1760 cm^{-1} ($\Delta\nu_{NN}$ = 820 cm^{-1}). Additionally, the Wiberg bond index decreases from 3.029 to 1.278 (ΔWBI_{NN} = 1.751), indicating a transformation of the N−N bond strength from a triple-bond character to a delocalized single-bond character,

https://doi.org/10.1021/acs.inorgchem.5c00726
Inorg. Chem. 2025, 64, 10115−10126

consistent with the bond length and frequency analyses. Most notably, the hydroboration of $\mathbf{P1}_{\mathbf{NCN7R}}$ can achieve N_2 activation to an even greater extent. Specifically, the formation of 1,1-hydroboration product $\mathbf{P3}_{\mathbf{NCN7R}}$ results in an elongation of the N−N bond length by 0.262 Å, a decrease in the vibration frequency by 1345 cm^{-1}, and a reduction in the WBI by 1.930. This outcome can be attributed to the "push−pull" electronic effect formed by the introduction of HB, which facilitates further N_2 activation. As shown in Figure 6, the NPA

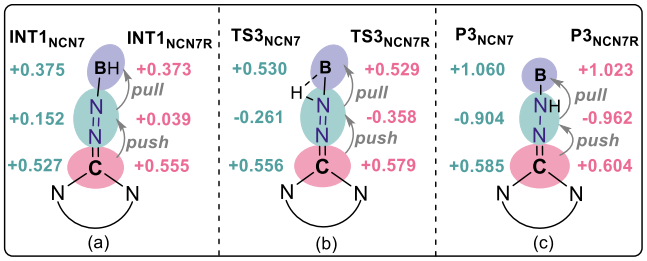

Figure 6. NPA of key intermediates (a), transition states (b), and products (c) in the hydroboration process.

indicates that during the hydroboration process, the carbene "pushes" electrons toward the N_2 fragment (the NPA charge change on the N_2 unit is +0.039 → −0.358 → −0.962e), while the HB "pulls" electrons toward the boron unit, with the NPA charge on the boron atom changing from +0.373 to +0.529 to +1.023e, suggesting a "Carbene → N_2 → BH" push−pull electronic effect. Compared to $\mathbf{TS3}_{\mathbf{NCN7}}$ (−0.261e), the N_2 fragment in $\mathbf{TS3}_{\mathbf{NCN7R}}$ receives more electrons (−0.358e), indicating that more significant electron transfer is beneficial for the kinetics of the 1,1-hydroboration of the η^1-N_2-type product. This finding aligns with our previous findings.[65]

To gain a deeper understanding of the differences in activation energies for N_2 activation by $\sigma^2\pi^0$-configured carbenes **NCN7** and **NCN7R**, we conducted an energy decomposition analysis (EDA)[89] on the transition states $\mathbf{TS1}_{\mathbf{NCN7}}$ and $\mathbf{TS1}_{\mathbf{NCN7R}}$ (as shown in Table S2). The computational results indicate that the higher deformation energy of the carbene (ΔE_{deform}(carbene): +6.3 kcal/mol vs +3.9 kcal/mol) is the primary reason for the destabilization of $\mathbf{TS1}_{\mathbf{NCN7}}$ compared to $\mathbf{TS1}_{\mathbf{NCN7R}}$. Additionally, the slightly lower binding energy between the deformed reactants (ΔE_b: −0.5 kcal/mol vs −1.3 kcal/mol) contributes to the greater stability of $\mathbf{TS1}_{\mathbf{NCN7R}}$. Moreover, the deformation energy of N_2 ($\Delta E_{deform}(N_2)$: +0.1 kcal/mol vs +0.1 kcal/mol) is negligible, indicating that the N_2 fragment undergoes virtually no deformation. This observation is supported by the nearly unchanged N≡N bond length in the geometric structures. Meanwhile, the analysis of $\mathbf{TS2}_{\mathbf{NCN7}}$ and $\mathbf{TS2}_{\mathbf{NCN7R}}$ involved in the bis-carbene functionalization process (as shown in Table S3) indicates that introducing another carbene molecule significantly contributes to the further stabilization of the η^1-N_2 adducts, with binding energies of −50.5 and −46.6 kcal/mol, respectively. However, the difference in deformation energy of the carbene fragment within the η^1-N_2 adducts [ΔE_{deform}(carbene′): +44.3 vs +26.2 kcal/mol] is the decisive factor for the barrier differences between $\mathbf{TS2}_{\mathbf{NCN7}}$ and $\mathbf{TS2}_{\mathbf{NCN7R}}$ (25.2 vs 16.6 kcal/mol). In summary, the above analyses suggest that the reaction barriers of the TSs during N_2 fixation and bis-carbene functionalization processes are primarily attributed to the deformation of the carbene. Further geometric structure analysis (as illustrated in Figures 5 and S10) shows that the total changes in important bond lengths ($\sum\Delta$BL, as shown in Figure S11) corresponding to each step's transition state follow the order: $\mathbf{TS1}_{\mathbf{NCN7R}}$ < $\mathbf{TS1}_{\mathbf{NCN7}}$ (0.093Å < 0.138 Å) and $\mathbf{TS2}_{\mathbf{NCN7R}}$ < $\mathbf{TS2}_{\mathbf{NCN7}}$ (0.450 Å < 0.542 Å). Simultaneously, the extent of change in the ∠N−C−N angle within **NCN7R** is always less than that observed in **NCN7**. However, it is noteworthy that although the change in the ∠C−N−N angle in $\mathbf{TS2}_{\mathbf{NCN7R}}$ is significantly greater than that in $\mathbf{TS2}_{\mathbf{NCN7}}$ (30.9 > 5.2°), this structural distortion contributes to the stabilization of the transition state to some extent. Specifically, as shown in Figure 7, the real-space function IRI analysis, which clearly reveals chemical bonds and weak interactions, indicates significant van der Waals interactions between the interacting fragments in $\mathbf{TS2}_{\mathbf{NCN7R}}$. In contrast, $\mathbf{TS2}_{\mathbf{NCN7}}$ exhibits only slightly repulsive interactions. Similarly, as indicated in Figure 8, the EDA results for the hydroboration step show that the barrier differences between $\mathbf{TS3}_{\mathbf{NCN7}}$ and $\mathbf{TS3}_{\mathbf{NCN7R}}$ (27.3 vs 13.7 kcal/mol) are mainly attributed to the binding energies between the N_2-carbene adduct fragment and the HB fragment (−51.9 vs −68.7 kcal/mol). Further analysis, in Figure 8c,d, reveals that this difference originates from the HOMO−LUMO gap between interacting fragments (1.76 vs 0.81 eV). Thus, a smaller HOMO−LUMO gap between interacting fragments correlates with a more pronounced binding energy.

The PIO analysis, which can identify and quantify the major orbital interactions between two interacting fragments, clearly reveals that the coordination between the occupied and unoccupied p-orbitals of the carbene carbon atom is a critical reason for $\sigma^2\pi^0$-configured carbenes achieving N_2 activation. As

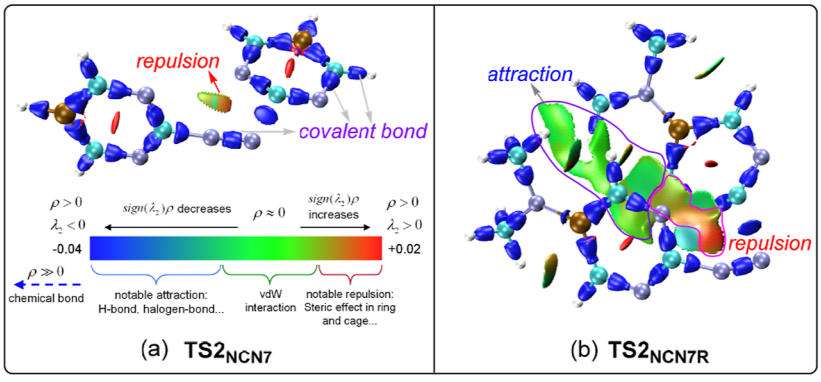

Figure 7. IRI analysis of $\mathbf{TS2}_{\mathbf{NCN7}}$ (a) and $\mathbf{TS2}_{\mathbf{NCN7R}}$ (b) (isovalue = 1.0 au).

https://doi.org/10.1021/acs.inorgchem.5c00726
Inorg. Chem. 2025, 64, 10115−10126

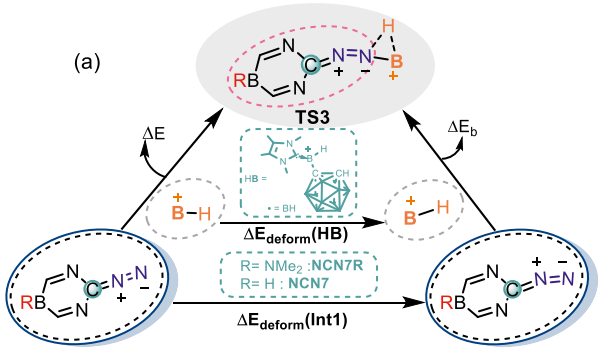

(b)

Entry	ΔE_b	ΔE_{deform} (HB)	ΔE_{deform} (Int1)	ΔE (barrier) [a]
$TS3_{NCN7}$	-51.9	1.7	26.5	-23.7
$TS3_{NCN7R}$	-68.7	0.1	26.5	-42.0

[a] $\Delta E(barrier) = \Delta E_{deform}(HB) + \Delta E_{deform}(Int1) + \Delta E_b$

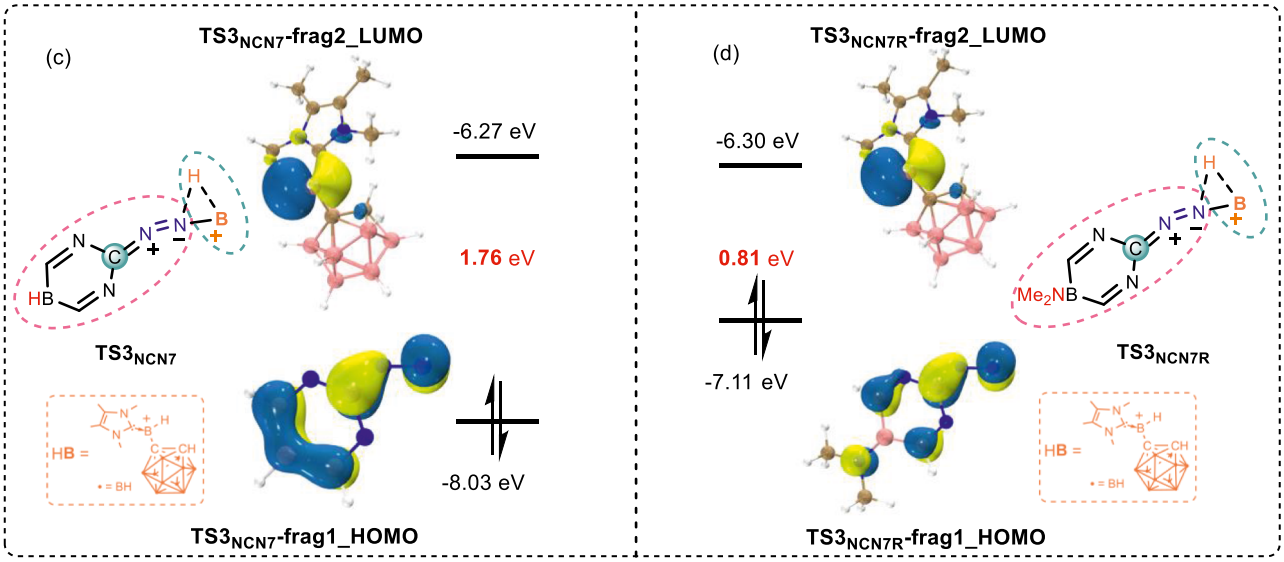

Figure 8. EDA of the N_2 hydroboration of transition states ($TS3_{NCN7}$ and $TS3_{NCN7R}$). (a) The general formula for EDA calculation and the corresponding results (b). The electronic energies are given in kcal/mol. Frontier molecular orbitals for the fragments of $TS3_{NCN7}$ (c) and $TS3_{NCN7R}$ (d) (isovalue = 0.05).

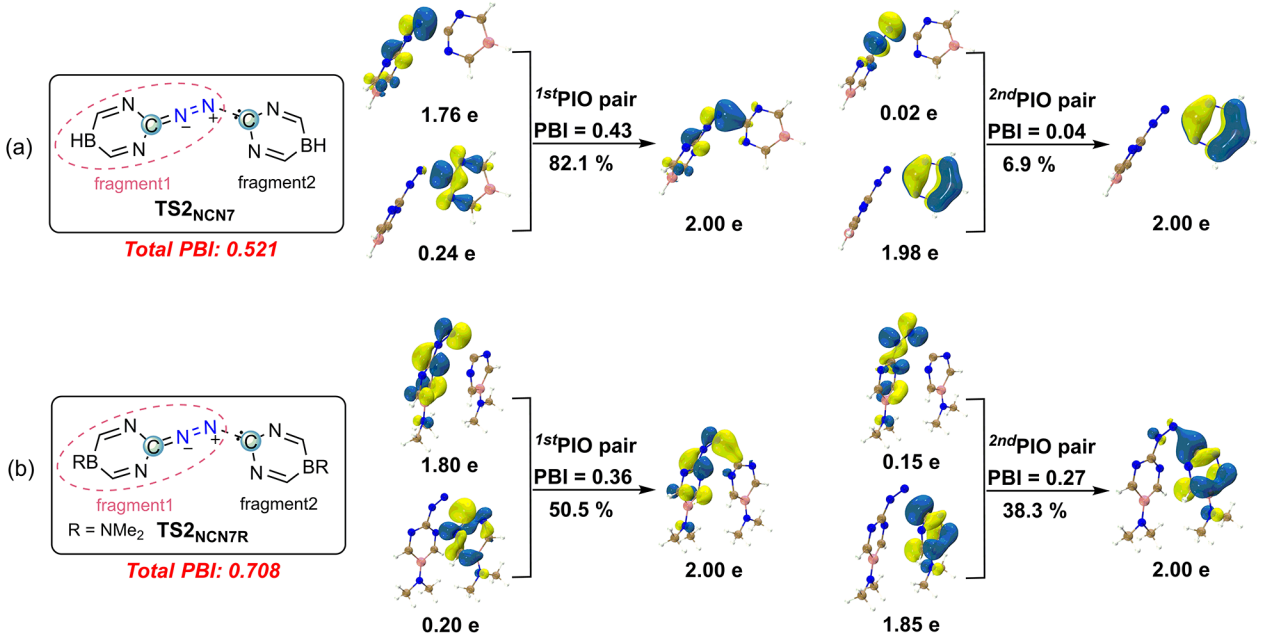

Figure 9. PIO analysis of $TS2_{NCN7}$ (a) and $TS2_{NCN7R}$ (b). The population (pop) of each PIO and the PIO-based bond index (PBI) and the percentage contribution of each PIO pair are given here (isovalue = 0.05).

https://doi.org/10.1021/acs.inorgchem.5c00726
Inorg. Chem. 2025, 64, 10115−10126

shown in Figure S12, the first set of interactions between the interacting fragments in $\mathbf{TS1}_{\mathbf{NCN7}}$ involves $p(N_2) \rightarrow$ vacant $p(C)$, while the second set of PIO pairs involves p_π(carbene carbon) $\rightarrow \pi^*(N_2)$, with interaction strengths of PBI of 0.49 and 0.07, respectively. This indicates that electron transfer from the N_2 fragment to the σ-type sp^2-empty orbital of the carbene carbon is the primary interaction in the N_2 fixation step.[49,50] In comparison, although the interactions between the interacting fragments in $\mathbf{TS1}_{\mathbf{NCN7R}}$ are consistent with those of the parent compound, the corresponding interaction strengths of PBI are weakened, being 0.37 and 0.06, respectively. Furthermore, as illustrated in Figure 9, comparing the PIO analyses of $\mathbf{TS2}_{\mathbf{NCN7}}$ and $\mathbf{TS2}_{\mathbf{NCN7R}}$ reveals that while the first set of PIO pair interactions differs only slightly between the two (PBI values of 0.43 and 0.36), the difference in the second set of PIO pairs' PBI is significant at 0.23 (0.04 vs 0.27). Additionally, the electron occupancy numbers of the interacting fragments indicate that the newly introduced carbene fragment in $\mathbf{TS2}_{\mathbf{NCN7R}}$ contributes more significantly through its $2p_\pi$-orbitals, transferring more electrons to the antibonding $\pi^*(N_2)$ orbitals of the N_2 fragment. This increased the possibility that electron transfer into the antibonding orbitals of N_2 is key to N_2 activation.

In addition to N_2 activation, the $\sigma^2\pi^0$-configured carbene **CNC7R** can also achieve a series of H-X (X = H, CH_3, Bpin, SiH_2Ph) bond insertion reactions. Computational results indicate that the activation processes of these H-X bonds are both thermodynamically and kinetically favorable. As shown in Figure 10, the order of transition state barriers for the insertion

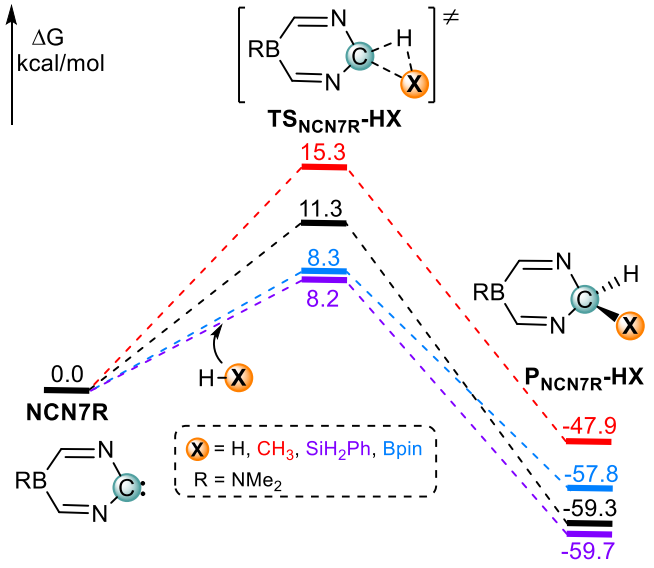

Figure 10. Gibbs energy (kcal/mol) profiles for H−X (X = H, CH_3, Bpin, SiH_2Ph) bond activation by $\sigma^0\pi^2$ carbene **CNC7R**.

of H-X bonds with **CNC7R** is as follows: H−CH_3 (15.3 kcal/mol) > H−H (11.3 kcal/mol) > H-Bpin (8.3 kcal/mol) > H-SiH_2Ph (8.2 kcal/mol). Further EDA calculation results (Table S4) show that the higher activation energy for methane (H−CH_3) is mainly attributed to the greater deformation energy of the reactants [ΔE_{deform}(carbene + H-X) = 13.2 kcal/mol], while the lowest reaction barrier for H-SiH_2Ph is primarily due to the binding energy between deformed reactants (ΔE_b: −6.5 kcal/mol) and $\pi-\pi$ interactions between aromatic rings of interacting fragments in the transition state (as illustrated in Figure S13). Additionally, as shown in Figure S14, the PIO analysis of the TSs for the activation processes indicates that the primary interactions between **CNC7R** and small molecules such as methane, hydrogen, HBpin, and SiH_3Ph are σ(H-X) → vacant p(C) and p_π(carbene carbon) → σ^*(H-X). Moreover, **NCN7R** is also highly sensitive to C−H bonds in some common solvents (Figure S15), such as benzene, cyclohexane, and tetrahydrofuran, highlighting the importance of selecting the appropriate solvents for this type of reaction. Similar N_2 activation pathways utilizing borylenes have been documented to compare with the C−H bond activation, notably in the work of Braunschweig et al.[24,30b]

Acyclic $\sigma^0\pi^2$ Carbenes. The computational results presented in Table 1 indicate that although the noncyclic $\sigma^0\pi^2$ carbene model molecule proposed by Wagner, **CCC1**, does not yield a thermodynamically favorable product upon bis-carbene-complexation with N_2, the formation of the η^1-N_2-type $\mathbf{P1}_{CCC1}$ is exothermic by 6.0 kcal/mol. Comparative calculations show that the triplet electronic state of **CCC1** has an electronic energy 9.0 kcal/mol lower than that of the singlet state. Consequently, we computed the kinetic processes for both distinct electronic states. As illustrated in Figure S16, the reaction barrier for the singlet state is lower than that for the triplet state, being 20.6 and 37.9 kcal/mol, respectively. This suggests that after the triplet ground-state **CCC1** interacts with N_2 via noncovalent interactions, it transitions through the minimum energy crossing point to the singlet state, overcoming an activation energy of 20.6 kcal/mol to generate the singlet-state N_2 fixation product $\mathbf{P1}_{CCC1}$. It is similar to the previous findings of Miliordos et al.[49] In contrast, the extremely high reaction barrier along the triplet-state pathway is not kinetically favorable. To further explore the activation and transformation of coordinated N_2, the 1,1-hydroboration reaction was computationally investigated. As indicated by the blue path in Figure S16, introducing the HB^a leads to its coordination with $\mathbf{P1}_{CCC1}$, forming intermediate $\mathbf{INT1}_{CCC1}{}^a$. This is followed by a transition through $\mathbf{TS2}_{CCC1}{}^a$ ($\Delta G^{\neq}$ = 99.5 kcal/mol) to form $\mathbf{P2}_{CCC1}{}^a$, which is endergonic by 47.3 kcal/mol, indicating that this process is both thermodynamically and kinetically highly unfavorable. Subsequently, another Lewis acid, HB^b [$HB(C_6F_5)_2$], was attempted, as shown by the cyan path in Figure S16. Unfortunately, while $HB(C_6F_5)_2$ can achieve further stabilization of the η^1-N^2-type product, resulting in a thermodynamically stable intermediate $\mathbf{INT1}_{CCC1}{}^b$ (ΔG = −11.4 kcal/mol), the reaction barrier that spans $\mathbf{TS2}_{CCC1}{}^b$ ($\Delta G^{\neq}$ = 29.2 kcal/mol) remains significant, which makes the process challenging to achieve and would require higher temperatures in experimental settings.

$\sigma^2\pi^0$ Carbenes. To further elucidate the strong potential of $\sigma^0\pi^2$ carbenes in N_2 activation, we compared their reactivity with that of the commonly used cyclic (alkyl)(amino)carbene (CAAC) toward N_2. As shown in Figure S17, mechanistic calculations indicate that while the process of assisting N_2 bis-carbene-functionalization by CAAC is thermodynamically favorable, the exceedingly high reaction barriers ($\Delta G_{TS1}^{\neq}$ = 44.1 kcal/mol and $\Delta G_{TS2}^{\neq}$ = 52.2 kcal/mol) suggest that such transformations are virtually unachievable under mild conditions. Furthermore, as shown in Figures S12 and S18, the PIO analysis uncovered that the interaction strength between the sp^2-lone-pair in $\sigma^2\pi^0$ carbenes (CAAC) and the π^* antibonding orbitals of N_2 is significantly greater compared to the backdonation of $\sigma^0\pi^2$ carbenes with N_2 (0.64 vs 0.06). Concurrently, the shorter C···N distances in the transition

https://doi.org/10.1021/acs.inorgchem.5c00726
Inorg. Chem. 2025, 64, 10115−10126

states further indicate stronger repulsion between the bonding atoms ($\mathbf{TS1}_{NCN7R}$ > $\mathbf{TS1}_{NCN7}$ > $\mathbf{TS1}_{CAAC}$:1.975 Å > 1.850 Å > 1.575 Å), which is consistent with our previous studies.[60,90] Additionally, in Figure S19, frontier orbital analysis indicates that the lower LUMO of the $\sigma^0\pi^2$ carbene may be a critical reason for its greater propensity to interact with the highest occupied molecular orbital of N_2.

CONCLUSION

In summary, we systematically investigated the potential of cyclic and acyclic $\sigma^0\pi^2$-configured carbenes in assisting the hydroboration and bis-carbene functionalization of N_2 using density functional theory calculations. Among these species, **NCN7R** (R = NMe_2) is considered the most likely candidate for experimental synthesis, as it exhibits optimal kinetic and thermodynamic properties. The reaction barriers for both processes are as low as 13.7 and 16.6 kcal/mol, respectively. Detailed mechanistic studies reveal that $\sigma^0\pi^2$-configured carbenes can effectively activate nitrogen by utilizing their unoccupied and occupied p orbitals to achieve a synergistic interaction of electron acceptance and electron donation. Surprisingly, introducing a Lewis acid **HB** at the terminal nitrogen atom of the η^1-N_2-type complex $\mathbf{P1}_{NCN7R}$ creates a "push−pull" electronic effect, further stabilizing it. Subsequent 1,1-hydroboration reactions exhibit superior thermodynamics (−57.8 vs −44.0 kcal/mol) and kinetics (13.7 vs 16.6 kcal/mol) compared to those of the bis-carbene-complexation process of N_2. Evidence of N_2 activation includes elongated N−N bonds (increased by 0.262 Å), reduced stretching vibration frequencies (decreased by 1345 cm^{-1}), and a weakened WBI (1.930). Additionally, EDA analysis reveals that the lower deformation energy of carbenes contributes to the favorable kinetics of **NCN7R** in N_2 activation. Moreover, **NCN7R** can also facilitate a series of X−H insertion reactions (X = H, CH_3, Bpin, SiH_2Ph), with activation energies as low as 8.2 to 15.3 kcal/mol. Our findings underscore the strong potential of carbenes with a $\sigma^0\pi^2$ electronic configuration in N_2 activation and its versatile transformations, providing valuable insights into metal-free N_2 activation chemistry.

ASSOCIATED CONTENT

Supporting Information

The Supporting Information is available free of charge at https://pubs.acs.org/doi/10.1021/acs.inorgchem.5c00726.

Cartesian coordinates of all stationary points located in this work (PDF)

AUTHOR INFORMATION

Corresponding Author

Jun Zhu − *School of Science and Engineering, The Chinese University of Hong Kong, Shenzhen, Guangdong 518172, China*; orcid.org/0000-0002-2099-3156; Email: jun.zhu@cuhk.edu.cn

Authors

Shicheng Dong − *State Key Laboratory of Physical Chemistry of Solid Surfaces, Fujian Provincial Key Laboratory of Theoretical Computational Chemistry, Department of Chemistry, College of Chemistry and Chemical Engineering, Xiamen University, Xiamen 361005, China*; orcid.org/0000-0001-9309-762X

Jun Yan − *School of Science and Engineering, The Chinese University of Hong Kong, Shenzhen, Guangdong 518172, China*; orcid.org/0000-0001-9966-4357

Weitang Li − *School of Science and Engineering, The Chinese University of Hong Kong, Shenzhen, Guangdong 518172, China*

Zhigang Shuai − *School of Science and Engineering, The Chinese University of Hong Kong, Shenzhen, Guangdong 518172, China*

Complete contact information is available at: https://pubs.acs.org/10.1021/acs.inorgchem.5c00726

Notes

The authors declare no competing financial interest.

ACKNOWLEDGMENTS

We acknowledge financial support from the National Natural Science Foundation of China (22073079), Shenzhen Science and Technology Program (Grant Nos. 2024SC0019 and KQTD20240729102028011), and the University Development Fund at the Chinese University of Hong Kong, Shenzhen (UDF01003116).

REFERENCES

(1) Burgess, B. K.; Lowe, D. J. Mechanism of molybdenum nitrogenase. *Chem. Rev.* **1996**, *96*, 2983−3012.

(2) Chalkley, M. J.; Drover, M. W.; Peters, J. C. Catalytic N_2-to-NH_3 (or -N_2H_4) conversion by well-defined molecular coordination complexes. *Chem. Rev.* **2020**, *120*, 5582−5636.

(3) Hoffman, B. M.; Lukoyanov, D.; Yang, Z.-Y.; Dean, D. R.; Seefeldt, L. C. Mechanism of nitrogen fixation by nitrogenase: The next stage. *Chem. Rev.* **2014**, *114*, 4041−4062.

(4) Schlögl, R. Ammonia Synthesis. In *Handbook of Homogeneous Catalysis*; Ertl, G., Knözinger, H., Schüth, F., Weitkamp, J., Eds.; Wiley: New York, 2008; pp 100−120.

(5) Schlögl, R. Catalytic Synthesis of Ammonia - A "Never-Ending Story". *Angew. Chem., Int. Ed.* **2003**, *42*, 2004−2008.

(6) Chen, J. G.; Crooks, R. M.; Seefeldt, L. C.; Bren, K. L.; Bullock, R. M.; Darensbourg, M. Y.; Holland, P. L.; Hoffman, B.; Janik, M. J.; Jones, A. K.; Kanatzidis, M. G.; King, P.; Lancaster, K. M.; Lymar, S. V.; Pfromm, P.; Schneider, W. F.; Schrock, R. R. Beyond fossil fuel-driven nitrogen transformations. *Science* **2018**, *360*, No. eaar6611.

(7) Hidai, M.; Mizobe, Y. Recent advances in the chemistry of dinitrogen complexes. *Chem. Rev.* **1995**, *95*, 1115−1133.

(8) MacKay, B. A.; Fryzuk, M. D. Dinitrogen coordination chemistry: on the biomimetic borderlands. *Chem. Rev.* **2004**, *104*, 385−402.

(9) Schrock, R. R. Catalytic reduction of dinitrogen to ammonia at a single molybdenum center. *Acc. Chem. Res.* **2005**, *38*, 955−962.

(10) Burford, R. J.; Fryzuk, M. D. Examining the relationship between coordination mode and reactivity of dinitrogen. *Nat. Rev. Chem* **2017**, *1*, 0026.

(11) McWilliams, S. F.; Holland, P. L. Dinitrogen binding and cleavage by multinuclear iron complexes. *Acc. Chem. Res.* **2015**, *48*, 2059−2065.

(12) Burford, R. J.; Yeo, A.; Fryzuk, M. D. Dinitrogen activation by group 4 and group 5 metal complexes supported by phosphine-amido containing ligand manifolds. *Coord. Chem. Rev.* **2017**, *334*, 84−99.

(13) Singh, D.; Buratto, W. R.; Torres, J. F.; Murray, L. J. Activation of dinitrogen by polynuclear metal complexes. *Chem. Rev.* **2020**, *120*, 5517−5581.

(14) Kim, S.; Loose, F.; Chirik, P. J. Beyond ammonia: nitrogen-element bond forming reactions with coordinated dinitrogen. *Chem. Rev.* **2020**, *120*, 5637−5681.

(15) Forrest, S. J. K.; Schluschaß, B.; Yuzik-Klimova, E. Y.; Schneider, S. Nitrogen Fixation via Splitting into Nitrido Complexes. *Chem. Rev.* **2021**, *121*, 6522−6587.
(16) Lv, Z.-J.; Wei, J.; Zhang, W.-X.; Chen, P.; Deng, D.; Shi, Z.-J.; Xi, Z. Direct transformation of dinitrogen: synthesis of N-containing organic compounds via N-C bond formation. *Natl. Sci. Rev.* **2020**, *7*, 1564−1583.
(17) (a) Shima, T.; Hu, S.; Luo, G.; Kang, X.; Luo, Y.; Hou, Z. Dinitrogen cleavage and hydrogenation by a trinuclear titanium polyhydride complex. *Science* **2013**, *340*, 1549−1552. (b) Zhuo, Q.; Yang, J.; Zhou, X.; Shima, T.; Luo, Y.; Hou, Z. Dinitrogen Cleavage and Multicoupling with Isocyanides in a Dititanium Dihydride Framework. *J. Am. Chem. Soc.* **2024**, *146*, 10984−10992. (c) Eberle, L.; Ballmann, J. Synthesis of Collidine from Dinitrogen via a Tungsten Nitride. *J. Am. Chem. Soc.* **2024**, *146*, 7979−7984. (d) Zhang, G.; Li, Q.; Wang, X.; Jin, L.; Liao, Q. Diverse Behaviors of N_2 on Mo Centers Bearing POCOP-Pincer Ligands and the Role of π-Electron Configuration in Regulating the Pathway of N_2 Activation. *J. Am. Chem. Soc.* **2025**, *147*, 3747−3757.
(18) Melen, R. L. A step closer to metal-free dinitrogen activation: a new chapter in the chemistry of frustrated Lewis pairs. *Angew. Chem., Int. Ed.* **2018**, *57*, 880−882.
(19) Broere, D. L.; Holland, P. L. Boron compounds tackle dinitrogen. *Science* **2018**, *359*, 871.
(20) Légaré, M. A.; Pranckevicius, C.; Braunschweig, H. Metallomimetic Chemistry of Boron. *Chem. Rev.* **2019**, *119*, 8231−8261.
(21) Hering-Junghans, C. Metal-free nitrogen fixation at boron. *Angew. Chem., Int. Ed.* **2018**, *57*, 6738−6740.
(22) (a) Liu, T.-T.; Zhai, D.-D.; Guan, B.-T.; Shi, Z.-J. Nitrogen fixation and transformation with main group elements. *Chem. Soc. Rev.* **2022**, *51*, 3846−3861. (b) Li, L.; Tang, C.; Jin, H.; Davey, K.; Qiao, S.-Z. Main-group Elements Boost Electrochemical Nitrogen Fixation. *Chem.* **2021**, *7*, 3232−3255.
(23) Soleilhavoup, M.; Bertrand, G. Cyclic (Alkyl)(Amino)Carbenes (CAACs): Stable Carbenes on the Rise. *Acc. Chem. Res.* **2015**, *48*, 256−266.
(24) Légaré, M. A.; Bélanger-Chabot, G.; Dewhurst, R. D.; Welz, E.; Krummenacher, I.; Engels, B.; Braunschweig, H. Nitrogen fixation and reduction at boron. *Science* **2018**, *359*, 896−900.
(25) Légaré, M. A.; Rang, M.; Bélanger-Chabot, G.; Schweizer, J. I.; Krummenacher, I.; Bertermann, R.; Arrowsmith, M.; Holthausen, M. C.; Braunschweig, H. The Reductive Coupling of Dinitrogen. *Science* **2019**, *363*, 1329−1332.
(26) Légaré, M. A.; Bélanger-Chabot, G.; Rang, M.; Dewhurst, R. D.; Krummenacher, I.; Bertermann, R.; Braunschweig, H. One-pot, room-temperature conversion of dinitrogen to ammonium chloride at a main-group element. *Nat. Chem.* **2020**, *12*, 1076−1080.
(27) Walawalkar, M. G. Boron: the first p-block element to fix inert N_2 all the way to NH_3. *Dalton Trans.* **2021**, *50*, 460−465.
(28) Hussain, Z.; Luo, Y.-A.; Wu, Y.; Qu, Z. w.; Grimme, S.; Stephan, D. W. Diazene Chemistry: Metal-Free Models of N_2 Reduction Intermediates. *J. Am. Chem. Soc.* **2023**, *145*, 7101−7106.
(29) (a) Rang, M.; Fantuzzi, F.; Arrowsmith, M.; Krummenacher, I.; Beck, E.; Witte, R.; Matler, A.; Rempel, A.; Bischof, T.; Radacki, K.; Engels, B.; et al. Reduction and Rearrangement of a Boron(I) Carbonyl Complex. *Angew. Chem., Int. Ed.* **2021**, *60*, 2963−2968. (b) Gärtner, A.; Karaca, U. S.; Rang, M.; Heinz, M.; Engel, P. D.; Krummenacher, I.; Arrowsmith, M.; Hermann, A.; Matler, A.; Rempel, A.; Witte, R.; Braunschweig, H.; Holthausen, M. C.; Légaré, M.-A. Achieving Control over the Reduction/Coupling Dichotomy of N_2 by Boron Metallomimetics. *J. Am. Chem. Soc.* **2023**, *145*, 8231−8241. (c) Rang, M.; Heinz, M.; Halkić, A.; Weber, M.; Dewhurst, R. D.; Rempel, A.; Härterich, M.; Holthausen, M. C.; Braunschweig, H. Trapping of a Terminal Intermediate in the Boron-Mediated Dinitrogen Reduction: Mono-, Tri-, and Tetra-functionalized Hydrazines in Two Steps from N_2. *J. Am. Chem. Soc.* **2024**, 11048−11053.
(30) (a) Zhang, H.; Yuan, R.; Wu, W.; Mo, Y. Two push-pull channels enhance the dinitrogen activation by borylene compounds. *Chem.—Eur. J.* **2020**, *26*, 2520. (b) You, F.; Zeng, J.; Rouf, A. M.; Dong, S.; Zhu, J. Theoretical study on reaction mechanisms of dinitrogen activation and coupling by carbene-stabilized borylenes in comparison with intramolecular C-H bond activation. *Chem.—Asian J.* **2022**, *17*, No. e202200232. (c) Fantuzzi, F.; Moral, R.; Dewhurst, R. D.; Braunschweig, H.; Phukan, A. K. Probing the potential of hitherto unexplored base-stabilized borylenes in dinitrogen binding. *Chem.—Eur. J.* **2022**, *28*, No. e202104123. (e) Zeng, J.; Su, J.; You, F.; Zhu, J. Understanding reaction mechanisms of metal-free dinitrogen activation by methyleneboranes. *Chin. Chem. Lett.* **2023**, *34*, 107759.
(31) Deng, G.; Pan, S.; Wang, G.; Zhao, L.; Zhou, M.; Frenking, G. Side-on bonded beryllium dinitrogen complexes. *Angew. Chem., Int. Ed.* **2020**, *59*, 10603−10609.
(32) Rösch, B.; Gentner, T. X.; Langer, J.; Färber, C.; Eyselein, J.; Zhao, L.; Ding, C.; Frenking, G.; Harder, S. Dinitrogen complexation and reduction at low-valent calcium. *Science* **2021**, *371*, 1125−1128.
(33) Mondal, R.; Evans, M. J.; Rajeshkumar, T.; Maron, L.; Jones, C. Coordination and Activation of N_2 at Low-Valent Magnesium using a Heterobimetallic Approach: Synthesis and Reactivity of a Masked Dimagnesium Diradical. *Angew. Chem., Int. Ed.* **2023**, *62*, No. e202308347.
(34) Xu, B.; Beckers, H.; Ye, H.; Lu, Y.; Cheng, J.; Wang, X.; Riedel, S. Cleavage of the N≡N triple bond and unpredicted formation of the cyclic 1,3-diaza-2,4-diborete $(FB)_2N_2$ from N_2 and fluoroborylene BF. *Angew. Chem., Int. Ed.* **2021**, *60*, 17205−17210.
(35) Edel, K.; Krieg, M.; Grote, D.; Bettinger, H. F. Photoreactions of phenylborylene with dinitrogen and carbon monoxide. *J. Am. Chem. Soc.* **2017**, *139*, 15151−15159.
(36) Bennaamane, S.; Rialland, B.; Khrouz, L.; Fustier-Boutignon, M.; Bucher, C.; Clot, E.; Mézailles, N. Ammonia Synthesis at Room Temperature and Atmospheric Pressure from N_2: A Boron-Radical Approach. *Angew. Chem., Int. Ed.* **2023**, *62*, No. e202209102.
(37) Dumas, J. B.; Peligot, E. Annales de chimie et de physique. *Ann. Chim. Phys.* **1835**, No. 58, 5−74.
(38) von E Doering, W.; Hoffmann, A. K. The Addition of Dichlorocarbene to Olefins. *J. Am. Chem. Soc.* **1954**, *76*, 6162−6165.
(39) (a) Igau, A.; Grutzmacher, H.; Baceiredo, A.; Bertrand, G. Analogous α,α'-bis-carbenoid triply bonded species: synthesis of a stable λ^3-phosphinocarbene-λ^5-phosphaacetylene. *J. Am. Chem. Soc.* **1988**, *110*, 6463−6466. (b) Arduengo III, A. J.; Harlow, R. L.; Kline, M. A stable crystalline carbene. *J. Am. Chem. Soc.* **1991**, *113*, 361−363.
(40) (a) Enders, D.; Niemeier, O.; Henseler, A. Organocatalysis by N-Heterocyclic Carbenes. *Chem. Rev.* **2007**, *107*, 5606−5655. (b) Peris, E. Smart N-Heterocyclic Carbene Ligands in Catalysis. *Chem. Rev.* **2018**, *118*, 9988−10031. (c) Xia, Y.; Qiu, D.; Wang, J. Transition-Metal-Catalyzed Cross-Couplings through Carbene Migratory Insertion. *Chem. Rev.* **2017**, *117*, 13810−13889.
(41) (a) Zhukhovitskiy, A. V.; MacLeod, M. J.; Johnson, J. A. Carbene Ligands in Surface Chemistry: From Stabilization of Discrete Elemental Allotropes to Modification of Nanoscale and Bulk Substrates. *Chem. Rev.* **2015**, *115*, 11503−11532. (b) Smith, C. A.; Narouz, M. R.; Lummis, P. A.; Singh, I.; Nazemi, A.; Li, C. H.; Crudden, C. M. N. Heterocyclic Carbenes in Materials Chemistry. *Chem. Rev.* **2019**, *119*, 4986−5056.
(42) (a) Oehninger, L.; Rubbiani, R.; Ott, I. N-Heterocyclic carbene metal complexes in medicinal chemistry. *Dalton Trans.* **2013**, *42*, 3269−3284. (b) Liu, W.; Gust, R. Update on metal N-heterocyclic carbene complexes as potential anti-tumor metallodrugs. *Coord. Chem. Rev.* **2016**, *329*, 191−213.
(43) Moore, C. B.; Pimentel, G. C. Matrix Reaction of Methylene with Nitrogen to Form Diazomethane. *J. Phys. Chem.* **1964**, *41*, 3504−3509.
(44) Shilov, A. E.; Shteinman, A. A.; Tjabin, M. B. Reaction of carbenes with molecular nitrogen. *Tetrahedron Lett.* **1968**, *9*, 4177−4180.
(45) (a) Wilson, T. B.; Kistiakowsky, G. B. Reactions of Methylene. III. Addition to Carbon Monoxide. *J. Am. Chem. Soc.* **1958**, *80*, 2934−

2939. (b) Braun, W.; Bass, A. M.; Pilling, M. Flash Photolysis of Ketene and Diazomethane: The Production and Reaction Kinetics of Triplet and Singlet Methylene. *J. Chem. Phys.* **1970**, *52*, 5131−5143. (c) Eder, T. W.; Carr, R. W. Collision-Induced Singlet→Triplet Intersystem Crossing of Methylene and Methylene-d_2. *J. Chem. Phys.* **1970**, *53*, 2258−2266. (d) Herzberg, G. Molecular Spectra and Molecular Structure III. In *Electronic Spectra and Electronic Structure of Polyatomic Molecules*; D. Van Nostrand Co. Inc: New York, 1966.

(46) Grieve, D. M. A.; Lewis, G. E.; Ravenscroft, M. D.; Skrabal, P.; Sonoda, T.; Szele, I.; Zollinger, H. Reactivity of Carbenes and Related Compounds towards Molecular Nitrogen. *Helv. Chim. Acta* **1985**, *68*, 1427−1443.

(47) Liu, M. T. H.; Choe, Y.-K.; Kimura, M.; Kobayashi, K.; Nagase, S.; Wakahara, T.; Niino, Y.; Ishitsuka, M. O.; Maeda, Y.; Akasaka, T. Effect of Substituents on the Thermal Decomposition of Diazirines: Experimental and Computational Studies. *J. Org. Chem.* **2003**, *68*, 7471−7478.

(48) Park, S.; Chun, Y.; Cho, S. J.; Lee, S.; Kim, K. S. Design of carbene-based organocatalysts for nitrogen fixation: theoretical study. *J. Chem. Theory Comput.* **2012**, *8*, 1983−1988.

(49) Khan, S. N.; Kalemos, A.; Miliordos, E. Metal-Free Activation of N_2 by Persistent Carbene Pairs: An Ab Initio Investigation. *J. Phys. Chem. C* **2019**, *123*, 21548−21553.

(50) (a) Kirkland, J. K.; Johnson, S. K.; Vogiatzis, K. D. Computational investigation of functionalized carbenes on dinitrogen activation. *J. Comput. Chem.* **2023**, *44*, 832−842. (b) Papakondylis, A.; Mavridis, A. A Theoretical Investigation of the Structure and Bonding of Diazomethane, CH_2N_2. *J. Phys. Chem. A* **1999**, *103*, 1255−1259. (c) Papakondylis, A.; Mavridis, A. Accurate Structural Parameters and Binding Energy of the X^1A_1 State of Diazomethane Through Coupled-Cluster Calculations. *Chem. Phys. Lett.* **2014**, *600*, 103−105.

(51) Song, H.; Lee, E. Theoretical assessment of dinitrogen fixation on carbon atom. *Chem.—Asian J.* **2021**, *16*, 2421−2425.

(52) (a) Welch, G. C.; Juan, R. R. S.; Masuda, J. D.; Stephan, D. W. Reversible, Metal-Free Hydrogen Activation. *Science* **2006**, *314*, 1124. (b) Stephan, D. W.; Erker, G. Frustrated Lewis Pair Chemistry: Development and Perspectives. *Angew. Chem., Int. Ed.* **2015**, *54*, 6400−6441. (c) Stephan, D. W. The broadening reach of frustrated Lewis pair chemistry. *Science* **2016**, *354*, aaf7229. (d) Stephan, D. W. Catalysis, FLPs, and Beyond. *Chem.* **2020**, *6*, 1520−1526.

(53) Zhu, J. Rational design of a carbon-boron frustrated Lewis pair for metal-free dinitrogen activation. *Chem.—Asian J.* **2019**, *14*, 1413−1417.

(54) Rouf, A. M.; Huang, Y.; Dong, S.; Zhu, J. Systematic design of a frustrated Lewis pair containing methyleneborane and carbene for dinitrogen activation. *Inorg. Chem.* **2021**, *60*, 5598−5606.

(55) Rouf, A. M.; Dai, C.; Xu, F.; Zhu, J. Dinitrogen activation by tricoordinated boron species: a systematic design. *Adv. Theory Simul.* **2020**, *3*, 1900205.

(56) Rouf, A. M.; Dai, C.; Dong, S.; Zhu, J. Screening borane species for dinitrogen activation. *Inorg. Chem.* **2020**, *59*, 11770−11781.

(57) Dai, C.; Huang, Y.; Zhu, J. Predicting dinitrogen activation by carborane-based frustrated Lewis pairs. *Organometallics* **2022**, *41*, 1480−1487.

(58) Dai, C.; Zhu, J. Predicting dinitrogen activation by borenium and borinium cations. *Phys. Chem. Chem. Phys.* **2022**, *24*, 14651−14657.

(59) Dong, S.; Zhu, J. Predicting Small Molecule Activation including Catalytic Hydrogenation of Dinitrogen Promoted by a Dual Lewis Acid. *Chem.—Asian J.* **2022**, *18*, No. e202200991.

(60) Dong, S.; Zhu, J. Predicting Small Molecule Activations Including Dinitrogen Based on an Inorganic Benzene B_4N_2 Framework. *Inorg. Chem.* **2024**, *63*, 15984−15992.

(61) Maier, G.; Endres, J. 2H-Imidazole-2-ylidene: New Insights from a Matrix-Spectroscopic Study. *Chem.—Eur. J.* **1999**, *5*, 1590−1597.

(62) Chen, B.; Rogachev, A. Y.; Hrovat, D. A.; Hoffmann, R.; Borden, W. T. How to Make the $\sigma^0\pi^2$ Singlet the Ground State of Carbenes. *J. Am. Chem. Soc.* **2013**, *135*, 13954−13964.

(63) (a) Ruiz, J.; Mosquera, M. E. G.; Garcia, G.; Patrón, E.; Riera, V.; García-Granda, S.; Van der Maelen, F. Trapping Highly Electrophilic Metalladiphosphanylcarbenes. *Angew. Chem., Int. Ed.* **2003**, *42*, 4767−4771. (b) Vignolle, J.; Gornitzka, H.; Maron, L.; Schoeller, W. W.; Bourissou, D.; Bertrand, G. Transient Palladadiphosphanylcarbenes: Singlet Carbenes with an "Inverse" Electronic Configuration ($p\pi^2$ instead of σ^2) and Unusual Transannular Metal−Carbene Interactions ($\pi_{C\rightarrow Pd}$ Donation and $\sigma_{Pd\rightarrow C}$ Back-donation). *J. Am. Chem. Soc.* **2007**, *129*, 978−985. (c) Shibutani, Y.; Kusumoto, S.; Nozaki, K. Synthesis, Characterization, and Trapping of a Cyclic Diborylcarbene, an Electrophilic Carbene. *J. Am. Chem. Soc.* **2023**, *145*, 16186−16192.

(64) Hu, C.; Wang, X.-F.; Li, J.; Chang, X.-Y.; Liu, L. L. A stable rhodium-coordinated carbene with a $\sigma^0\pi^2$ electronic configuration. *Science* **2024**, *383*, 81−85.

(65) Dong, S.; Zhu, J. Predicting Activation of Small Molecules Including Dinitrogen via a Carbene with a $\sigma^0\pi^2$ Electronic Configuration. *Inorg. Chem.* **2024**, *63*, 15931−15940.

(66) (a) Wang, C. H.; Yin, Z. B.; Wei, J. N.; Zhang, W. X.; Xi, Z. Outlook of nitrogen fixation by carbene. *Tetrahedron* **2020**, *76*, 131703. (b) Tang, C.; Liang, Q.; Jupp, A. R.; Johnstone, T. C.; Neu, R. C.; Song, D.; Grimme, S.; Stephan, D. W. 1,1-Hydroboration and a Borane Adduct of Diphenyldiazomethane: A Potential Prelude to FLP-N_2 Chemistry. *Angew. Chem., Int. Ed.* **2017**, *56*, 16588−16592.

(67) (a) Zhao, Y.; Truhlar, D. G. Density functionals with broad applicability in chemistry. *Acc. Chem. Res.* **2008**, *41*, 157−167. (b) Zhao, Y.; Truhlar, D. G. The M06 suite of density functionals for main group thermochemistry, thermochemical kinetics, noncovalent interactions, excited states, and transition elements: two new functionals and systematic testing of four M06-class functionals and 12 other functionals. *Theor. Chem. Acc.* **2008**, *120*, 215−241.

(68) (a) Yang, H.; Wong, M. W. Oxyanion hole stabilization by C−H···O interaction in a transition state-a three-point interaction Model for cinchona alkaloid-catalyzed asymmetric methanolysis of meso-cyclic anhydrides. *J. Am. Chem. Soc.* **2013**, *135*, 5808−5818. (b) Kikuchi, J.; Aramaki, H.; Okamoto, H.; Terada, M. F_{10}BINOL-derived chiral phosphoric acid-catalyzed enantioselective carbonyl-ene reaction: theoretical elucidation of stereochemical outcomes. *Chem. Sci.* **2019**, *10*, 1426−1433. (c) Guo, J.; Wong, M. W. Cinchona alkaloid-squaramide catalyzed Sulfa-Michael addition reaction: mode of bifunctional activation and origin of stereoinduction. *J. Org. Chem.* **2017**, *82*, 4362−4368.

(69) Frisch, M. J.; Trucks, G. W.; Schlegel, H. B.; Scuseria, G. E.; Robb, M. A.; Cheeseman, J. R.; Scalmani, G.; Barone, V.; Petersson, G. A.; Nakatsuji, H.; Li, X.; Caricato, M.; Marenich, A. V.; Bloino, J.; Janesko, B. G.; Gomperts, R.; Mennucci, B.; Hratchian, H. P.; Ortiz, J. V.; Izmaylov, A. F.; Sonnenberg, J. L.; Williams; Ding, F.; Lipparini, F.; Egidi, F.; Goings, J.; Peng, B.; Petrone, A.; Henderson, T.; Ranasinghe, D.; Zakrzewski, V. G.; Gao, J.; Rega, N.; Zheng, G.; Liang, W.; Hada, M.; Ehara, M.; Toyota, K.; Fukuda, R.; Hasegawa, J.; Ishida, M.; Nakajima, T.; Honda, Y.; Kitao, O.; Nakai, H.; Vreven, T.; Throssell, K.; Montgomery, J. A., Jr; Peralta, J. E.; Ogliaro, F.; Bearpark, M. J.; Heyd, J. J.; Brothers, E. N.; Kudin, K. N.; Staroverov, V. N.; Keith, T. A.; Kobayashi, R.; Normand, J.; Raghavachari, K.; Rendell, A. P.; Burant, J. C.; Iyengar, S. S.; Tomasi, J.; Cossi, M.; Millam, J. M.; Klene, M.; Adamo, C.; Cammi, R.; Ochterski, J. W.; Martin, R. L.; Morokuma, K.; Farkas, O.; Foresman, J. B.; Fox, D. J. *Gaussian 16*. Revision A.03; Gaussian, Inc.: Wallingford CT, 2016.

(70) (a) Grimme, S.; Antony, J.; Ehrlich, S.; Krieg, H. A consistent and accurate*ab initio*parametrization of density functional dispersion correction (DFT-D) for the 94 elements H-Pu. *J. Chem. Phys.* **2010**, *132*, 154104. (b) Grimme, S.; Ehrlich, S.; Goerigk, L. Effect of the damping function in dispersion corrected density functional theory. *J. Comput. Chem.* **2011**, *32*, 1456−1465.

(71) Weigend, F.; Ahlrichs, R. Balanced basis sets of split valence, triple zeta valence and quadruple zeta valence quality for H to Rn: Design and assessment of accuracy. *Phys. Chem. Chem. Phys.* **2005**, *7*, 3297−3305.

https://doi.org/10.1021/acs.inorgchem.5c00726
Inorg. Chem. 2025, 64, 10115−10126

(72) Fukui, K. Formulation of the reaction coordinate. *J. Phys. Chem.* **1970**, *74*, 4161−4163.
(73) Fukui, K. The path of chemical reactions - the IRC approach. *Acc. Chem. Res.* **1981**, *14*, 363−368.
(74) Perdew, J. P. Density-functional approximation for the correlation energy of the inhomogeneous electron gas. *Phys. Rev. B* **1986**, *33*, 8822−8824.
(75) Becke, A. D. Density-functional exchange-energy approximation with correct asymptotic behavior. *Phys. Rev. A* **1988**, *38*, 3098−3100.
(76) Wiberg, K. B. Application of the pople-santry-segal CNDO method to the cyclopropylcarbinyl and cyclobutyl cation and to bicyclobutane. *Tetrahedron* **1968**, *24*, 1083−1096.
(77) Zhang, J. X.; Sheong, F. K.; Lin, Z. Unravelling chemical interactions with principal interacting orbital analysis. *Chem.—Eur. J.* **2018**, *24*, 9639−9650.
(78) Zhang, J. X.; Sheong, F. K.; Lin, Z. Principal interacting orbital: a chemically intuitive method for deciphering bonding interaction. *Wiley Interdiscip. Rev.: Comput. Mol. Sci.* **2020**, *10*, No. e1469.
(79) Glendening, E. D.; Badenhoop, J. K.; Reed, A. E.; Carpenter, J. E.; Bohmann, J. A.; Morales, C. M.; Karafiloglou, P.; Landis, C. R.; Weinhold, F. *NBO 7.0. Theoretical Chemistry Institute*; University of Wisconsin: Madison, WI, 2018; . http://nbo7.chem.wisc.edu/.
(80) Chen, Z.; Wannere, C. S.; Corminboeuf, C.; Puchta, R.; Schleyer, P. v. R. Nucleus-Independent Chemical Shifts (NICS) as an Aromaticity Criterion. *Chem. Rev.* **2005**, *105*, 3842−3888.
(81) Geuenich, D.; Hess, K.; Köhler, K.; Herges, R. Anisotropy of the induced current density (ACID), a general method to quantify and visualize electronic delocalization. *Chem. Rev.* **2005**, *105*, 3758−3772.
(82) Legault, C. Y. *CYLview*, ver. 1.0b. Université de Sherbrooke, 2009. http://www.cylview.org.
(83) Humphrey, W.; Dalke, A.; Schulten, K. VMD: Visual molecular dynamics. *J. Mol. Graphics* **1996**, *14*, 33−38.
(84) Lu, T.; Chen, Q. Interaction Region Indicator (IRI): A Simple Real Space Function Clearly Revealing Both Chemical Bonds and Weak Interactions. *Chem.:Methods* **2021**, *1*, 231−239.
(85) Lu, T.; Chen, F. Multiwfn a multifunctional wavefunction analyzer. *J. Comput. Chem.* **2012**, *33*, 580−592.
(86) Wagner, J. P. Designing a $\sigma^0\pi^2$ singlet ground state carbene from dicationic carbones. *Chem. Commun.* **2024**, *60*, 3327−3330.
(87) (a) Tan, X.; Wang, H. Recent advances in borenium catalysis. *Chem. Soc. Rev.* **2022**, *51*, 2583−2600. (b) Tan, X.; Wang, H. Borenium-Ions in Catalytic Aromatic C-H Borylation. *ChemCatChem* **2023**, *15*, No. e2023007. (c) Xu, Y.; Yang, Y.; Liu, Y.; Li, Z.; Wang, H. Boron-catalysed hydrogenolysis of unactivated C(aryl)−C(alkyl) bonds. *Nat. Catal.* **2023**, *6*, 16−22.
(88) (a) Simonneau, A.; Turrel, R.; Vendier, L.; Etienne, M. Group 6 transition-metal/boron frustrated Lewis pair templates activate N_2 and allow its facile borylation and silylation. *Angew. Chem., Int. Ed.* **2017**, *56*, 12268−12272. (b) Geri, J. B.; Shanahan, J. P.; Szymczak, N. K. Testing the push-pull hypothesis: Lewis acid augmented N_2 activation at iron. *J. Am. Chem. Soc.* **2017**, *139*, 5952−5956. (c) Yin, Z. B.; Wang, G. X.; Yan, X.; Wei, J.; Xi, Z. Construction of N−E bonds via Lewis acid-promoted functionalization of chromium-dinitrogen complexes. *Nat. Commun.* **2025**, *16*, 674.
(89) (a) Bickelhaupt, F. M.; Houk, K. N. Analyzing reaction rates with the distortion/interaction-activation strain model. *Angew. Chem., Int. Ed.* **2017**, *56*, 10070−10086. (b) Phipps, M. J.; Fox, T.; Tautermann, C. S.; Skylaris, C. K. Energy decomposition analysis approaches and their evaluation on prototypical protein-drug interaction patterns. *Chem. Soc. Rev.* **2015**, *44*, 3177−3211.
(90) Zhuang, D.; Li, Y.; Zhu, J. Antiaromaticity-Promoted Activation of Dihydrogen with Borole Fused Cyclooctatetraene Frustrated Lewis Pairs: A Density Functional Theory Study. *Organometallics* **2020**, *39*, 2636−2641.

https://doi.org/10.1021/acs.inorgchem.5c00726
Inorg. Chem. 2025, 64, 10115−10126